JOURNAL OF CATALYSIS **177,** 314–324 (1998)
ARTICLE NO. CA982123

Spectroscopic Studies on Tetragonal ZrO_2-Supported MoO_3 and NiO–MoO_3 Systems

Zheng Liu and Yi Chen[1]

Department of Chemistry, Institute of Mesoscopic Solid State Chemistry, Nanjing University, Nanjing 210093, China

Received October 24, 1997; revised March 20, 1998; accepted April 27, 1998

XRD, laser Raman, and UV–visible DR spectroscopies are used to study tetragonal zirconia-supported MoO_3 and NiO–MoO_3 oxide systems. For the MoO_3/t-ZrO_2 system, the results indicate that the distorted surface monomolybdate and polymolybdate species are the main species formed in the low and high MoO_3 loading samples, respectively. Crystalline MoO_3 is formed above its dispersion capacity, and at temperatures $\geq$823 K the supported MoO_3 species are partially converted into $ZrMo_2O_8$ phase by interaction with tetragonal zirconia (t-ZrO_2). Noteworthily, for the t-ZrO_2-supported binary oxides system, i.e., the NiO–MoO_3/t-ZrO_2 system, the species formed on the surface of the t-ZrO_2 depend on the loading sequence of the metal oxides. Depositing NiO before MoO_3 leads to the formation of a $NiMoO_4$ phase, whereas there is no evidence to show the presence of this phase when MoO_3 was added first. The results suggest that molybdenum oxide can substitute and react with the nickel oxide species predispersed on the surface of the zirconia with the formation of a new phase. In contrast, nickel oxide can only disperse by the incorporation of Ni^{2+} ions into the unoccupied vacant sites on the surface of the support preloaded with molybdenum oxide and interact with the polymolybdate species resulting in the formation of a surface interaction species. The experimentally measured dispersion capacities of MoO_3 and NiO on various supports, i.e., on t-ZrO_2, and MoO_3 or NiO-modified supports, are consistent with the values expected according to the incorporation model. The results emphasize the importance of the surface structure of the support and the calcination temperature on the dispersion of oxide and the formation of different surface species.

Key Words: **MoO_3; NiO; tetragonal ZrO_2; dispersion; interaction; Raman and UV–vis diffuse reflectance spectroscopes.**

INTRODUCTION

Supported molybdenum oxides catalysts are widely used in various catalytic processes (1). The molecular structures of the surface molybdenum oxide species on different oxide supports have been extensively investigated by various techniques (2). The conclusion is that the structures of the supported molybdenum oxide species are related to the nature, in particular the surface structure, of the support; the extent of surface hydration; the loading amount of molybdenum oxide; and the calcination temperatures (2–5). The structures of molybdenum oxide supported on γ-Al_2O_3 have been extensively studied under ambient conditions (6–12). Raman results (6–10) have demonstrated that at least three different molybdenum oxide species, i.e., tetrahedrally and octahedrally coordinated surface species as well as the crystalline MoO_3 phase, might be present on the surface of γ-Al_2O_3 and that their relative amounts depend on the loading of molybdenum oxide.

Several models concerning the interactions between supported molybdenum oxide and γ-Al_2O_3 have been proposed for the discussion of the dispersion states of the supported molybdenum oxide. As reviewed briefly (13), these models can tentatively be divided into two categories; i.e., the dispersed oxide species are spreading on the top of or incorporating into the surface of the support. One suggests that under appropriate conditions, the dispersed MoO_3 might cover the support with the formation of a monolayer on the top of the surface, and the other proposes that the dispersed Mo^{6+} cations might incorporate into the vacant sites on the surface of the support. Xie and Tang are the first to measure quantitatively the dispersion capacities of a series of metal oxides on γ-Al_2O_3 by XRD (14). The dispersion capacities of various ionic compounds on different supports have been measured and compared to the conclusions derived by different models. The close-packed monolayer model can explain the experimental data of MoO_3 and WO_3 oxides, but its discrepancies on predicting the dispersion capacities of metal oxides of lower valance types are obvious (14). On the other hand, the dispersion capacities of a series of ionic compounds on various supports derived by the incorporation model are consistent with the experimental data (13, 15–18). Moreover, the model predicts that the metal oxide of lower valence type, e.g., Li_2O, NiO, etc., cannot form a close-packed monolayer on the surface of the oxide supports even when its loading amount is as high as its dispersion capacity. Compared to the lower valence type oxides, MoO_3 and WO_3 are unique in that three anions accompany each cation, and a close-packed monolayer of oxygen anions can thus be formed on the top of the

[1] To whom correspondence should be addressed.

0021-9517/98 $25.00

incorporated Mo^{6+} or W^{6+} ions with a loading equal to its dispersion capacity.

It is known that metal oxide–oxide support interactions appreciably affect the surface properties of the supported oxide species, and hence the catalytic properties of them or their derivatives. Besides alumina considerable interest has now been devoted to other supports such as TiO_2, CeO_2, and ZrO_2 in exploring better catalysts through adjusting the interaction strength between the dispersed species and support. It has been reported that zirconia-supported Mo catalysts have higher activities in the HDS reaction of thiophene and in the hydrogenation of CO than the alumina-supported Mo catalysts (19), and for the partial oxidation of methanol (20) and ethanol (21) the high activities of catalysts of MoO_3 highly dispersed on ZrO_2 support have also been noted. However, in comparison to the MoO_3/γ-Al_2O_3 system, relatively few studies have been carried out on molybdenum oxides supported on ZrO_2 (21, 22), especially on tetragonal ZrO_2.

Mixed oxides, e.g., the combination of Mo, W, Co, or Ni oxides, supported on γ-Al_2O_3 are commonly used as precursors of catalysts for important reactions, such as hydrodesulfurization (HDS) or hydrodenitrogenation (HDN) in the petroleum industry. The characterization of these precursors has been greatly improved by the use of surface spectroscopic techniques. It has been found by ion scattering spectroscopy (ISS) that the MoO_3, CoO, and NiO phases are well dispersed on the surface of γ-Al_2O_3 (23, 24). The incorporation of the cobalt and nickel ions into the alumina support, at high temperatures, has been clearly detected even in the presence of MoO_3 phase in the NiO–MoO_3/γ-Al_2O_3 system (25). Dufresne *et al*. have investigated the above system with a constant MoO_3 loading of 14 wt% and the NiO loading is varied from 0.5 to 7.2 wt%; it is found by XPS and LRS (26) that for the low Ni^{2+} loading samples, the Ni^{2+} and Mo^{6+} species are well dispersed on γ-Al_2O_3 as two independent components without mutual interactions, whereas for the high Ni^{2+} loading samples a $NiMoO_4$ phase is formed. Ahuja *et al*. (27) have mentioned that for supported Mo and Co sulfide catalysts the dispersion extent of the oxides depends on the degree of the oxide–support interaction. Topsøe *et al*. (28) have also concluded that, for supported cobalt oxide catalysts, support plays an essential role in the formation of cobalt-containing phases in either oxide or sulfide states. Cheng and Schrader (29) have found that adding Co^{2+} before Mo^{6+} to the alumina support leads to the formation of a highly aggregated molybdenum species (trioxide) and that the order of the addition of the oxides is important. In contrast, Ng and Gulari (30) have claimed that on TiO_2 the surface molybdate species interact strongly with the support and the addition order of the molybdenum and cobalt oxides is not important. Adding cobalt to TiO_2-supported molybdenum oxide catalysts suppresses the formation of bulk MoO_3 and leads to the formation of a cobalt molybdate phase. Apparently, the state of the dispersed molybdenum oxide and promoter (Ni or Co) oxides depends on the nature of the support and the preparation method used. Thus it is interesting to further explore the effects of support and the preparation method on the state of molybdenum and promoter oxides dispersed on oxide supports besides alumina.

The objectives of this work are:

(1) to investigate the surface species formed in the t-ZrO_2-supported MoO_3 and NiO–MoO_3 systems, and the influence of the loading sequence of the oxides on their dispersion states by Raman and UV–visible DR spectroscopy;

(2) to compare the interactions between t-ZrO_2 and MoO_3 or NiO, and the interactions between the supported molybdenum and nickel oxides;

(3) to explore the effect of the surface structure of the support on the dispersion behavior of Mo and Ni oxides, and the effect of the calcination temperature on the state of the supported oxides species.

EXPERIMENTAL

Sample Preparation

Tetragonal zirconia (t-ZrO_2) was prepared by the method reported elsewhere (31). After being calcined at 773 K for 4 h, it has a BET surface area of 65 m^2/g.

Two MoO_3-modified t-ZrO_2 (designated as Mo_1Zr and Mo_2Zr) and two NiO-modified t-ZrO_2 (designated as Ni_1Zr and Ni_2Zr) samples were prepared by impregnating the t-ZrO_2 with aqueous solutions containing appropriate amounts of ammonium heptamolybdate or of nickel nitrate, respectively. After drying at 373 K for 16 h, the samples were then calcined in air at 773 K for 4 h. The amount of the metal oxide loadings in the above four modified t-ZrO_2 samples, i.e., on Mo_1Zr and Mo_2Zr, Ni_1Zr and Ni_2Zr, are 4.2 and 2.2 Mo^{6+} ions/nm^2 t-ZrO_2, and 8.5 and 4.2 Ni^{2+} ions/nm^2 t-ZrO_2, respectively.

Samples of MoO_3 and NiO supported on the different supports were prepared by impregnating each support with solution containing appropriate amounts of ammonium heptamolybdate or nickel nitrate, respectively, then dried at 373 K for 16 h and calcined in air at 773 K for 2 h. The loadings of the samples are listed below:

NiO/Mo_1Zr (Ni^{2+} ions/nm^2 t-ZrO_2):
(a) 2.5, (b) 4.5, (c) 7.0, and (d) 9.7.

NiO/Mo_2Zr (Ni^{2+} ions/nm^2 t-ZrO_2):
(a) 1.4, (b) 2.5, (c) 5.0, and (d) 8.4.

MoO_3/t-ZrO_2 (Mo^{6+} ions/nm^2 t-ZrO_2):
(a) 1.5, (b) 2.2, (c) 4.2, (d) 5.5, and (e) 10.

MoO_3/Ni_1Zr (Mo^{6+} ions/nm^2 t-ZrO_2):
(a) 2.3, (b) 4.8, (c) 7.5, and (d) 10.

MoO_3/Ni_2Zr (Mo^{6+} ions/nm^2 t-ZrO_2):
(a) 2.2, (b) 3.3, (c) 5.0, (d) 7.5, and (e) 10.

Sample Characterization

X-ray diffraction results were obtained by a Shimadzu XD-3A diffractometer with a Ni-filtered Cu$K\alpha$ radiation (1.5418 nm). The X-ray tube was operated at 35 kV and 20 mA, and XRD quantitative results were obtained using α-alumina powder as reference.

FT-laser Raman spectra were recorded by a Bruker RF-100 spectrometer with a wave number accuracy of 4 cm^{-1}. All the samples were measured in powder form and a Na:YAG crystal laser was used for excitation.

UV–visible diffuse reflectance spectra of the original and finely ground samples were recorded in the range of 200–800 nm by a Shimadzu UV-240 spectrophotometer with a $BaSO_4$ sample as reference.

RESULTS AND DISCUSSION

MoO_3/t-ZrO_2 System

Figure 1 shows the relationship of the amount of residual crystalline MoO_3 versus total MoO_3 content in the MoO_3/t-ZrO_2 samples as determined by XRD quantitative analysis. When the loading amounts of MoO_3 are low the highly dispersed molybdenum oxide species cannot be detected by XRD, and only when the loading amount exceeds a certain extent can the residual crystalline phase of MoO_3 be detected, as shown by the straight line in Fig. 1. The intercept of the straight line gives the dispersion capacity of MoO_3 on the t-ZrO_2, i.e., about 4.5 Mo^{6+} ions/nm^2 t-ZrO_2.

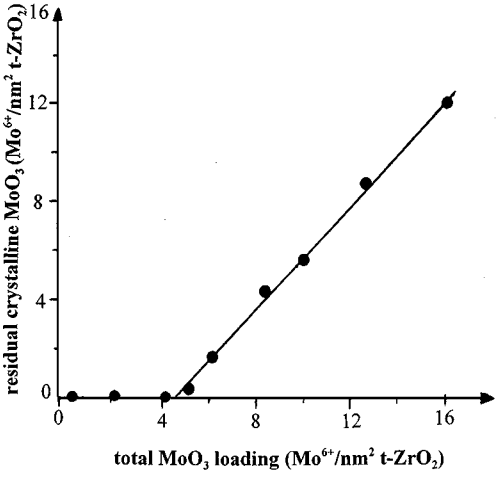

FIG. 1. XRD quantitative results on the amount of residual crystalline of MoO_3 vs its content in the supported samples calcined at 773 K.

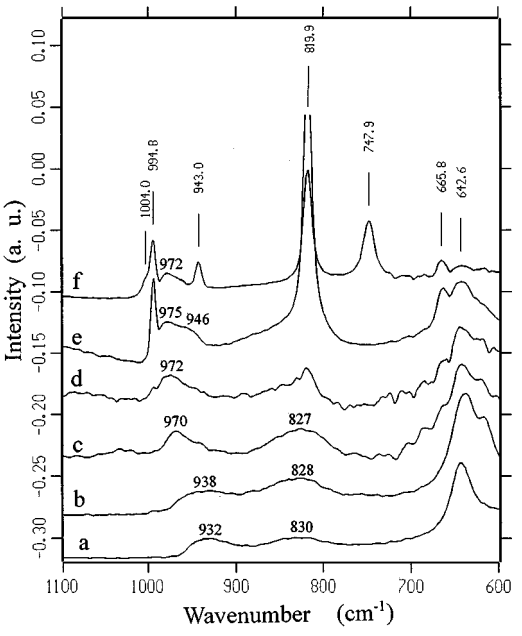

FIG. 2. Raman spectra of MoO_3/t-ZrO_2 samples with different amounts of MoO_3 loadings (Mo^{6+} ions/nm^2 t-ZrO_2): (a) 1.5, (b) 2.2, (c) 4.2, (d) 5.5, (e) 10, and (f) 10. Samples (a)–(e) are calcined at 773 K and (f) is calcined at 823 K.

Raman spectra have been used to characterize the dispersed molybdenum oxide species supported on various oxide supports such as γ-Al_2O_3 (6–10, 32, 33), TiO_2 (30, 32, 33), ZrO_2 (monoclinic) (21, 22, 32), MgO (33), and CeO_2 (34). Generally, monomolybdate or tetrahedral molybdenum–oxygen species have been assigned for low MoO_3 loading samples (26, 32), and two-dimensional polymolybdates or octahedral molybdenum–oxygen species with characteristic band around 950–980 cm^{-1} (26, 32), for high MoO_3 loading samples. Raman bands between 910 and 980 cm^{-1} are usually attributed to the Mo=O vibration of Mo species in either octahedral or tetrahedral environment (26). Shown in Fig. 2 is our Raman result of the MoO_3/t-ZrO_2 samples. Spectra with vibration frequencies below 600 cm^{-1} have not been collected due to the strong background of tetragonal zirconia. The band at 642 cm^{-1} is due to t-ZrO_2 (35) and its relative intensity decreases with the increase of MoO_3 loading. A broad band around 932 cm^{-1} is observed in the low MoO_3 loading samples (Figs. 2a and 2b), indicating the presence of monomolybdate species in these samples. As the MoO_3 loading increases, the terminal Mo=O stretching frequency shifts from 932 to 975 cm^{-1} which is assigned to the terminal Mo=O vibration of the polymolybdate species (36). The broad Raman band around 830 cm^{-1} is tentatively attributed to the Mo–O–Zr and/or Mo–O–Mo Raman stretching modes and no significant shift of this band position has been observed. Once the loading of MoO_3 reaches its dispersion capacity, the positions and intensities of the above two bands do not change with the further

increase of MoO_3 loading. The effect of the further addition of MoO_3 is the formation of crystalline MoO_3 in the spectrum as identified by its characteristic bands at 818 and 993 cm^{-1} (Figs. 2d and 2e). When the calcination temperature is raised to 823 K, a new species, i.e., $ZrMo_2O_8$ phase identified by its characteristic Raman bands at 748, 946, and 1003 cm^{-1} (37), has been detected in the high loading sample with 10 Mo^{6+} ions/nm^2 t-ZrO_2, as shown in Fig. 2f.

To discuss the nature of the dispersed species and the features of their Raman spectra, the interaction between the dispersed species and the support should be taken into consideration. It is known that tetragonal zirconia has a slightly distorted fluorite structure and only half of its distorted cube sites surrounded by oxygen anions are occupied by Zr^{4+} ions. With the assumption that (111) planes are preferentially exposed on the surface of the zirconia (38, 39), its surface vacant sites can be calculated to be 8.7 sites/nm^2 t-ZrO_2; i.e., the sites can be used for the incorporation of the dispersed cations according to the incorporation model (16). For MoO_3/t-ZrO_2 samples, as the calcination temperature (773 K) is apparently higher than the Tamman temperature of MoO_3 (534 K) (13), it seems reasonable to consider that the probability of the dismantlement of the MoO_3 bulk phase into ion pairs or molecules is high at the temperature of calcination. And the highly mobile Mo^{6+} ions thus formed might migrate and incorporate into the vacant sites available on the underlying surface of the t-ZrO_2. As each incorporated Mo^{6+} ion is accompanied by three-oxygen anions positioning on its top for charge compensation, the shielding effect of the accompanying oxygen anions will prevent part of the vacant sites from being occupied. Accordingly, when the loading amount of MoO_3 reaches its dispersion capacity only part of the surface vacant sites are occupied by the dispersed Mo^{6+} ions with the formation of a close-packed monolayer of capping oxygen anions on the surface of zirconia. Based on the above discussion, it can be estimated that the dispersion capacity of MoO_3 on the surface of t-ZrO_2 should be around 4.8 Mo^{6+} ions/nm^2 t-ZrO_2, which is in good agreement with the results measured by XRD and LRS.

Taking into consideration the structure of the dispersed Mo^{6+} species discussed above, it is suggested that one of the three capping oxygen anions might locate on the top of the incorporated Mo^{6+} ion with the formation of the terminal Mo=O bond. The other two capping oxygen anions might associate with the coordinately unsaturated neighboring Zr^{4+} ions leading to the establishment of linkages between the cations on the surface and the appearance of the weak broad band at 826–835 cm^{-1}. The oxygen anion of the terminal Mo=O bond is exposed to the ambient atmosphere and easily interacts with the moisture, resulting in the formation of hydrated surface species. When the loading of MoO_3 is low, only isolated molybdenum oxide species, or say monomolybdate species, exist on the surface of zirconia with their Raman band around 932 cm^{-1}. With the increase of the loading of MoO_3 more vacant sites are occupied, and polymerized molybdenum oxide species gradually show up due to the linkage or the combination of the neighboring monomolybdate species. In fact, the mono- or polymolybdate species, often referred to respectively as tetrahedral and octahedral species in the literature, formed on the surface are often irregularly distorted due to their strong interaction with the surface of support. The distortion and different extent of interaction among surface molybdenum-oxygen species should be responsible for the large width and big shift of the terminal Mo=O Raman stretching bands as compared with the spectra of corresponding species in solution.

The UV–visible DR spectra of MoO_3/t-ZrO_2 samples, as shown in Fig. 3, are helpful in identifying the structures of the molybdenum species dispersed on t-ZrO_2. Since Mo^{6+} has a d° electronic configuration, the only absorption due to the ligand–metal charge transfer transition (LMCT), O—Mo^{6+} is observed, which is expected in the range of 200–400 nm. As reported elsewhere (40, 41) that the absorption bands in 260–280 and 300–320 nm are assigned to the isolated molybdate and polymolybdate species, respectively. Therefore, it is probable that the absorption band at *ca.* 262 nm of the low MoO_3 loading samples shown in Fig. 3

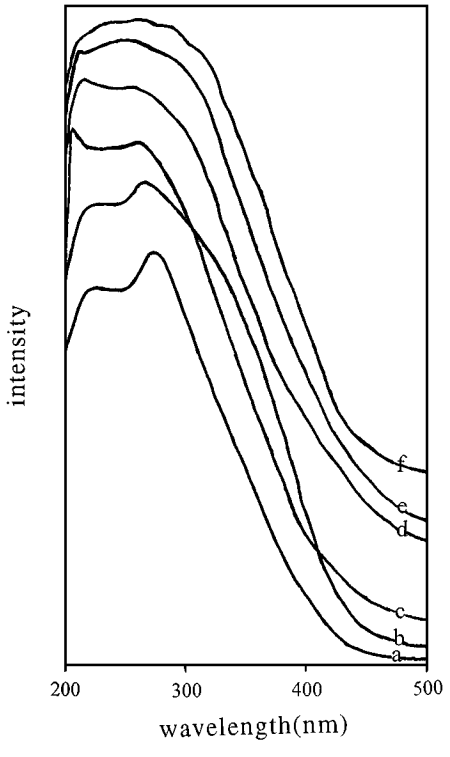

FIG. 3. UV–visible diffuse reflectance spectra of (a) $ZrMo_2O_8$ and (b)–(f) MoO_3/t-ZrO_2 samples with different amounts of MoO_3 loadings (Mo^{6+} ions/nm^2 t-ZrO_2): (b) 10, (c) 1.5, (d) 2.2, (e) 4.2, (f) 10. Samples (c)–(f) are calcined at 773 K and (b) is calcined at 823 K.

can be attributed to the isolated surface monomolybdate species. With the increase of Mo loading, a resolved band around 300 nm assigned tentatively to the surface polymolybdate species gradually becomes dominating. Finally, as can be seen in Fig. 3f, with the further increase of MoO_3 loading to a value higher than its dispersion capacity, i.e., 10 Mo^{6+}/nm^2 t-ZrO_2, a new shoulder around 335 nm is detected, suggesting the presence of bulk MoO_3 phase in the sample. The increase of the calcination temperature might promote the interaction between the residual MoO_3 phase and the support. In fact, after the above sample is calcined at 823 K for 2 h, it has a spectrum as shown in Fig. 3b, obviously different from that in Fig. 3f but similar to that of $ZrMo_2O_8$ (Fig. 3a), and the shoulder band around 335 nm in Fig. 3b indicates the coexistence of MoO_3 and $ZrMo_2O_8$.

MoO_3 on the NiO-Modified t-ZrO_2 Systems

It is well established that the addition of nickel to molybdenum oxide/alumina catalysts can improve their hydrodesulfurization activity significantly. Such a synergetic effect is believed to have a direct relation to the catalyst surface structure. In order to investigate the structure of the related surface oxide species formed on the zirconia and the interactions between the dispersed oxide species themselves and between the dispersed oxide species and support, samples of MoO_3 supported on NiO-modified t-ZrO_2 and samples of NiO supported on MoO_3-modified t-ZrO_2 are prepared and characterized. Reported in this section are results of samples of MoO_3 supported on two NiO-modified t-ZrO_2 supports, i.e., on Ni_1Zr and Ni_2Zr. The Ni^{2+} loading amount in Ni_1Zr is selected to be close to its dispersion capacity, i.e., 8.5 Ni^{2+} ions/nm^2 t-ZrO_2, while in Ni_2Zr the amount is about half that, namely, 4.2 Ni^{2+} ions/nm^2 t-ZrO_2. The Raman spectra of this series of samples calcined at 723 K are shown in Fig. 4. It is interesting to note that, as can be seen in Fig. 4c, even when the loading of MoO_3 is as low as 2.3 Mo^{6+} ions/nm^2 t-ZrO_2 it cannot disperse on Ni_1Zr, but under similar experimental conditions its dispersion on Ni_2Zr is obvious, as evidenced by Fig. 4a. It is apparent that the different surface structures of the two NiO-modified supports result in the different dispersion behaviors. As discussed in the previous section, the surface vacant sites on the (111) plane of the t-ZrO_2 are estimated to be 8.7 sites/nm^2 t-ZrO_2 and should be equal to the dispersion capacity of NiO on t-ZrO_2 according to the incorporation model. The expectation is in good agreement with the quantitative results of XRD, as shown in Fig. 5. With the picture of the incorporation of Ni^{2+} ions into the surface vacant sites in mind, the surface of the NiO-modified t-ZrO_2 sample is schematically shown in Fig. 6. It is evident that for the Ni_1Zr sample there are nearly no vacant sites left since its Ni^{2+} loading is 8.5 Ni^{2+}/nm^2 t-ZrO_2, an amount enough to fill almost all the vacant sites on the (111) plane of the t-ZrO_2. On the other hand, for Ni_2Zr support, there

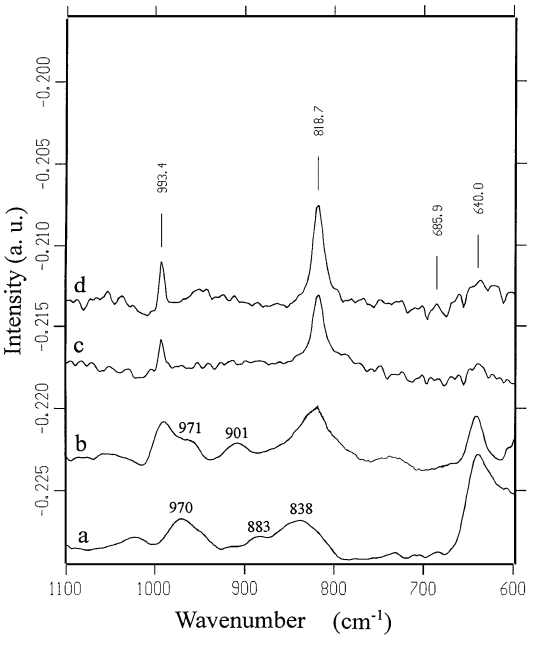

FIG. 4. Raman spectra of samples of MoO_3 supported on Ni_1Zr (c), (d) and Ni_2Zr calcined at 723 K with different amount of MoO_3 loadings (Mo^{6+} ions/nm^2 t-ZrO_2): (a) 2.2, (b) 5.0, (c) 2.3, and (d) 4.8.

are still surface vacant sites available for the incorporation of metal cations as its Ni^{2+} loading is only half that of Ni_1Zr. Consequently, the spectra of MoO_3 supported on Ni_2Zr, as shown in Figs. 4a and 4b, are more or less similar to those of MoO_3, supported on t-ZrO_2. The bands at 970 and 838 cm^{-1} of Fig. 4a indicate the formation of the surface polymolybdate species on this modified support. When the loading amount of MoO_3 exceeds its dispersion capacity, its

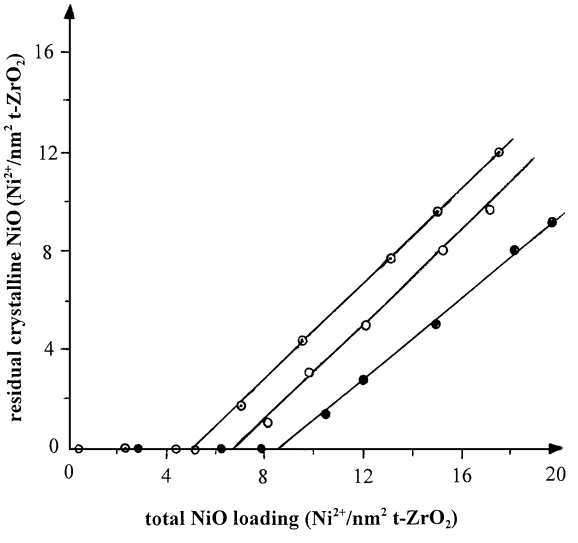

FIG. 5. Amount of residual NiO crystalline vs its content in samples of (●) NiO/t-ZrO_2, (⊙) NiO/Mo_1Zr, and (○) NiO/Mo_2Zr. Samples are calcined at 773 K.

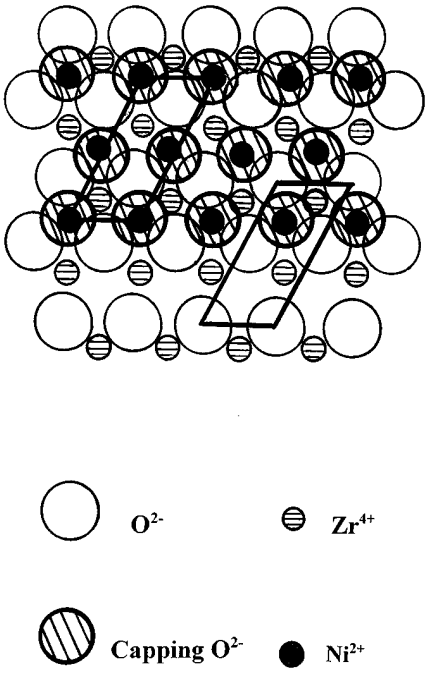

FIG. 6. A NiO-modified t-ZrO_2 (111) plane deduced from the incorporation model.

crystalline phase appears, as can be seen in Fig. 4b. No obvious evidence shows that there is any new phase formed by the interaction of the supported molybdenum species with either Ni_1Zr or Ni_2Zr calcined at 723 K.

Shown in Fig. 7 are the Raman spectra of MoO_3/Ni_1Zr samples with different MoO_3 loading calcined at a higher temperature, i.e., 773 K, under ambient conditions. A broad band around 970 cm^{-1} and a weak peak at 958 cm^{-1} overlapping on it are observed in Fig. 7a of the sample with a loading of 2.3 Mo^{6+} ions/nm^2 t-ZrO_2. The intensities of the sharp Raman band at 958 cm^{-1} and a new shoulder band at 946 cm^{-1} increase gradually with the increase of the loading of MoO_3. With reference to the spectrum of $NiMoO_4$ as shown in Fig. 7e, the presence of the sharp bands at 958 and 946 cm^{-1} reveals the existence of crystalline $NiMoO_4$ in this series of samples calcined at 773 K. XRD measurements have also supported the above conclusion by showing a diffraction peak at $2\theta = 26.7^\circ$ (42). Moreover, as the intensity of the broad band at 970 cm^{-1} also increases with the increase of the loading of MoO_3, it seems to suggest that the formation of $NiMoO_4$ phase and the polymerization of the surface molybdenum oxide species take place concurrently.

Referring to Figs. 4c and 4d and 7a and 7b, one can see that the dispersion of MoO_3 on Ni_1Zr support is promoted by the increase of the calcination temperature from 723 to 773 K. As all the vacant sites on Ni_1Zr are filled, a possible interpretation of the dispersion of MoO_3 on this support is that the thermal treatment at a higher temperature might promote the replacement of the incorporated Ni^{2+} ions by the dispersed Mo^{6+} ions and the interaction between them. Indeed as a result, the formation of a $NiMoO_4$ phase and the dispersion of MoO_3 are observed simultaneously. Further increase of the loading amount of MoO_3 leads to the formation of the residual crystalline MoO_3 coexisting with the $ZrMo_2O_8$ phase (751 cm^{-1}), as can be seen in Fig. 7d. The presence of a new $NiMoO_4$ phase implies that the interaction of the surface Ni^{2+} species with MoO_3 is stronger than that with the zirconia.

To further understand the influence of the surface structure of support on the dispersion state of MoO_3 and NiO, Raman spectra of MoO_3/Ni_2Zr series of samples calcined at 773 K are also measured and shown in Fig. 8. For samples with 2.2 and 3.3 Mo^{6+} ions/nm^2 t-ZrO_2, neither XRD nor LRS gives any evidence on the formation of $NiMoO_4$ phase, but the surface polymerized molybdenum species identified by the 971 cm^{-1} Raman band, as shown in Figs. 8a and 8b, are detected. The result is consistent with the fact that Ni_2Zr still has about half of its vacant sites that are not occupied by the incorporated Ni^{2+} ions and which can be used for the incorporation of the dispersed Mo^{6+} cations. The conclusion is then evident: the interaction of the supported MoO_3 with t-ZrO_2 is stronger than that with the dispersed Ni^{2+} species. Further increase of the loading amount of MoO_3 will finally lead to the formation of the $NiMoO_4$ and $ZrMo_2O_8$ phases as well as the crystalline MoO_3, as can be seen in Figs. 8b–8d.

The differences in Figs. 4a and 8a obtained from samples with the same low MoO_3 loading but calcined at different temperatures, i.e., at 723 and 773 K, respectively, should be attributed to the influence of calcination temperature on the

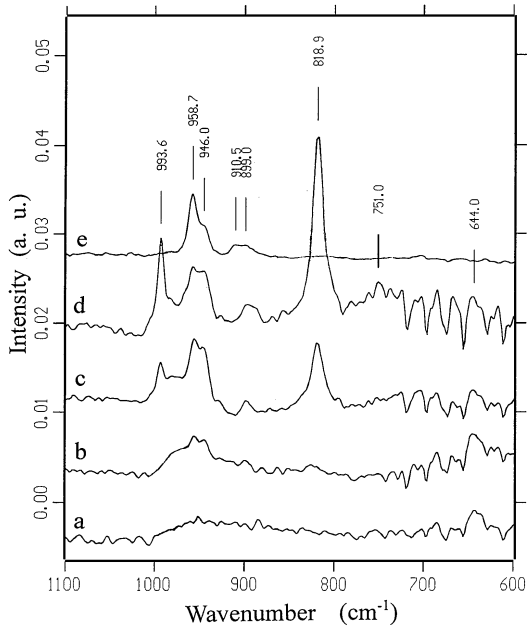

FIG. 7. Raman spectra of MoO_3/Ni_1Zr samples calcined at 773 K with different amounts of MoO_3 loadings (Mo^{6+} ions/nm^2 t-ZrO_2: (a) 2.3, (b) 4.8, (c) 7.5, (d) 10, and (e) $NiMoO_4$.

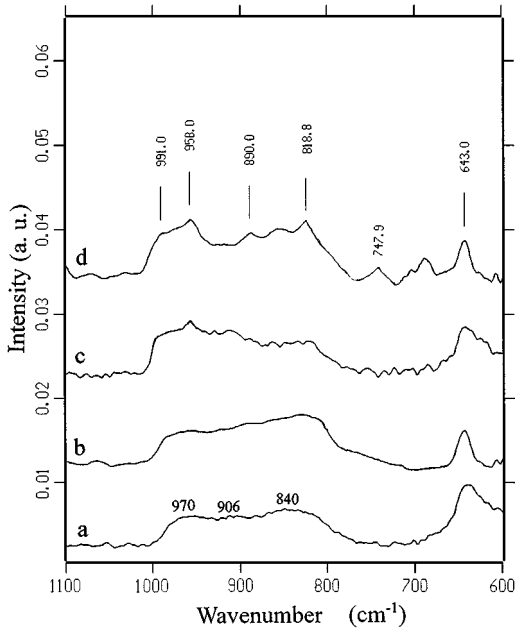

FIG. 8. Raman spectra of MoO_3/Ni_2Zr samples calcined at 773 K with different amounts of MoO_3 loadings (Mo^{6+} ions/nm^2 t-ZrO_2): (a) 2.2, (b) 3.3, (c) 5.0, and (d) 7.5.

dispersion and interaction of the oxide species. It is likely that the increase of the calcination temperature might promote the interactions between the dispersed nickel oxide and molybdenum oxide species themselves and between them and support. These kinds of interactions should be responsible for the broad band around 906 cm^{-1} in Fig. 8a, which has not been detected in Fig. 4a of the sample calcined at a lower temperature. To investigate the effect of calcination temperature on the high loading samples, laser Raman spectra of MoO_3 supported on Ni_1Zr and on Ni_2Zr samples with the same loading of 10 Mo^{6+} ions/nm^2 t-ZrO_2 but calcined at different temperatures are shown in Fig. 9. The influence of the calcination temperature is obvious but different in the MoO_3/Ni_1Zr and/or Ni_2Zr samples. The results of the MoO_3/Ni_1Zr are given in Fig. 9A. At temperatures below 773 K, i.e., 673 and 723 K, only MoO_3 crystalline phase is detected, and the result is reasonable, as on Ni_1Zr all the vacant sites are occupied and no sites are available for the incorporation of Mo^{6+} ions. To raise the calcination temperature to 773 K, as shown in the spectrum c of Fig. 9A, $NiMoO_4$ and $ZrMo_2O_8$ phases along with the surface dispersed molybdenum oxide species all appear in the sample, and the intensity of the characteristic peaks of crystalline MoO_3 decreases accordingly. Upon further increase of the calcination temperature to 823 K, as can be seen in the spectrum d of Fig. 9A, the amount of the $ZrMo_2O_8$ phase increases at the expense of that of crystalline MoO_3, and the Raman band at 958 cm^{-1} becomes more symmetric and sharp. For the case of MoO_3 supported on Ni_2Zr samples, Raman results are given in Fig. 9B. At calcination temperatures lower than 773 K, as shown in the spectra a, b of Fig. 9B, a broad band at 970 cm^{-1} indicating the existence of the polymolybdate species is formed by the incorporation of the Mo^{6+} into the surface vacant sites on Ni_2Zr. Noteworthily, the above polymeric Mo^{6+} species have not been detected in the Ni_1Zr-supported samples. To increase the calcination temperature to 773 K, the presence of a weak but sharp band at 958 cm^{-1} overlapping with the band at

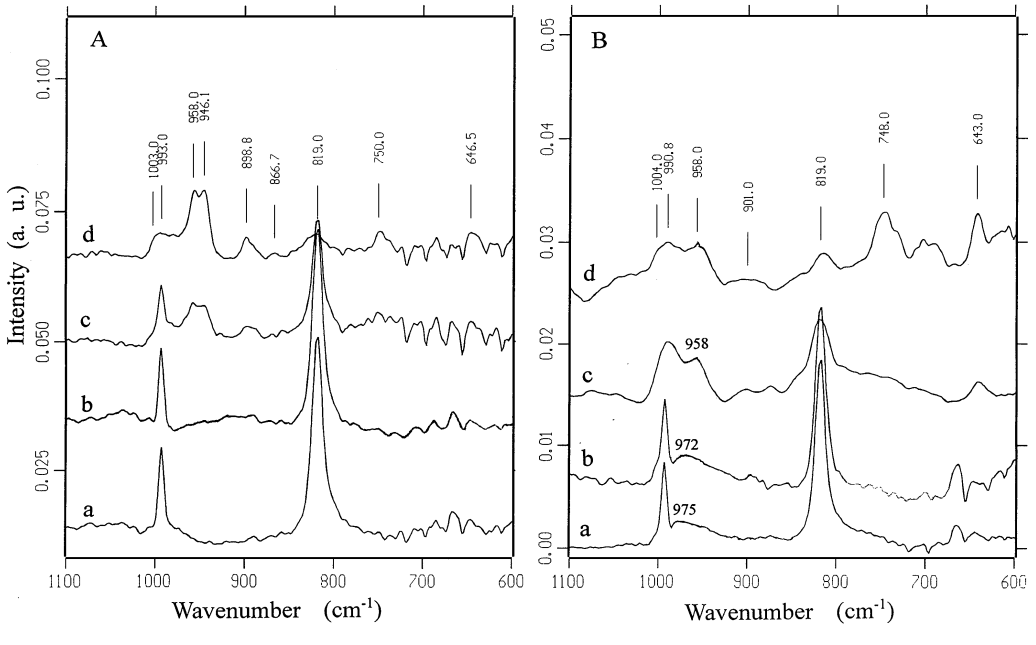

FIG. 9. Raman spectra of MoO_3/NiO-modified t-ZrO_2 samples with the same amount of MoO_3 loading of 10 Mo^{6+} ions/nm^2 t-ZrO_2. (A) MoO_3/Ni_1Zr and (B) MoO_3/Ni_2Zr calcined at different calcination temperatures (K): (a) 673, (b) 723, (c) 773 and (d) 823.

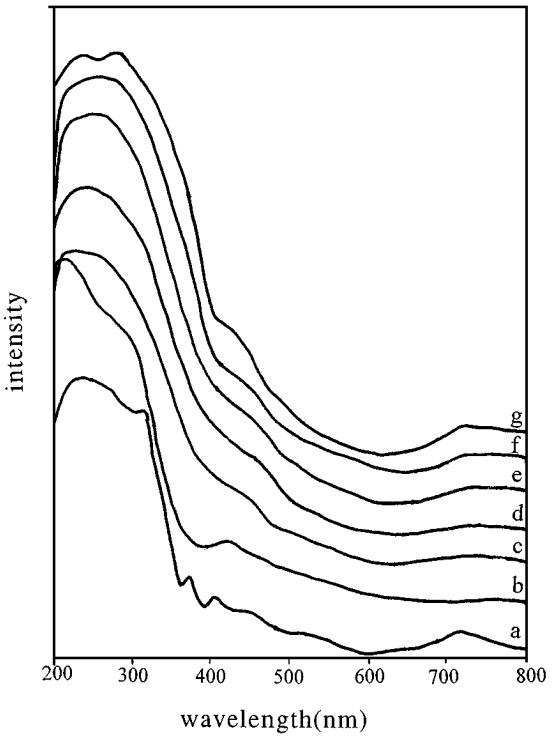

FIG. 10. UV–visible diffuse reflectance spectra of (a) NiO, (b) Ni_1Zr, (g) $NiMoO_4$, and (c)–(f) are MoO_3/Ni_1Zr samples calcined at 773 K with different amounts of MoO_3 loadings (Mo^{6+} ions/nm^2 t-ZrO_2): (c) 2.3, (d) 4.7, (e) 7.5, and (f) 10.

970 cm^{-1} indicates the formation of the $NiMoO_4$ phase. Almost all the residual MoO_3 phase is converted into the $ZrMo_2O_8$ phase at a calcination temperature of 823 K.

UV–visible diffuse reflectance spectra are measured to complement the Raman results. Shown in Fig. 10 are the DR spectra of MoO_3 supported on Ni_1Zr samples calcined at 773 K as well as the spectra of $NiMoO_4$, NiO and Ni_1Zr for comparison. For $NiMoO_4$, strong LMCT bands of Mo^{6+} (d°)/oxygen system at 230 and 280 nm are the typical characteristics of the tetrahedrally coordinated MoO_4 species. In the visible region, a band at 720 nm and a shoulder at about 420 nm of this spectrum have been assigned to the adsorption bands of octahedrally coordinated Ni^{2+} ions (7, 43). The above characterizations suggest that the Ni^{2+} and Mo^{6+} ions in $NiMoO_4$ are located in an octahedral environment and a tetrahedral environment, respectively. For the case of NiO, a strong ligand field transition at 405 nm has been assigned to the O_3 band ($^3A_{2g}$–$^3T_1(P)$) of Ni^{2+} ions in an octahedral environment (7, 43). In Ni_1Zr sample, as can be seen in Fig. 10b, most of the adsorption bands in the region of 350–800 nm detected in bulk NiO, e.g., bands at 385, 405, 560, and 456 nm, are replaced by a broad shoulder around 425 nm. The result suggests that the coordination environments of the Ni^{2+} ions in Ni_1Zr and in bulk NiO are apparently different, and the dispersed Ni^{2+} ions are probably positioned in a distorted polyhedral oxygen environment on the surface of t-ZrO_2 (44, 45). The DR spectra of MoO_3/Ni_1Zr samples with different MoO_3 loadings are shown in Figs. 10c–10f. The adsorption band around 425 nm of the Ni_1Zr sample becomes a weak and broad shoulder due to the addition of the MoO_3 species. Although the broad band is weak, it is clearly visible in the DR spectra of this series of samples. It should be noted that with the increase of the loading amount of MoO_3, the intensity of the broad band around 720 nm increases and the shape of the spectrum gradually becomes close to that of the $NiMoO_4$ sample. These results are consistent with the Raman results discussed above which suggest the formation of the $NiMoO_4$ phase through the interaction of the supported MoO_3 and Ni_1Zr. Similar conclusions can be drawn from the DR spectra of MoO_3/Ni_2Zr samples, which are not listed here.

NiO on MoO_3-Modified t-ZrO_2 Systems

To investigate the influence of the loading sequence on the nature of the supported binary oxides system, samples of NiO on the two MoO_3-modified t-ZrO_2 supports, i.e., Mo_1Zr (4.2 Mo^{6+} ions/nm^2t-ZrO_2) and Mo_2Zr (2.2 Mo^{6+} ions/nm^2 t-ZrO_2), are characterized. For the NiO/Mo_1Zr samples, the XRD results indicate that no $NiMoO_4$ phase can be detected but NiO still can disperse on this modified support with a dispersion capacity of 4.8 Ni^{2+} ions/nm^2 t-ZrO_2 as shown in Fig. 5. It is known that on Mo_1Zr, 4.2 sites/nm^2 t-ZrO_2 are occupied by the incorporated Mo^{6+} ions with the formation of a close-packed monolayer of the capping oxygen anions on the top. Consequently, there are about 4.5 sites/nm^2 t-ZrO_2 which remain unoccupied. It is interesting to see that the measured dispersion capacity of Ni^{2+} ions is so close to the number of unoccupied vacant sites on Mo_1Zr. The results seem to suggest that the thermal treatment at 773 K leads to the migration of Ni^{2+} ions across the oxygen capping layer and to their incorporation into the unoccupied surface vacant sites on t-ZrO_2. Thus addition of NiO might induce the structural reorganization of the surface molybdenum species because of the dispersion of Ni^{2+} ions around them. Shown in Fig. 11 are the Raman spectra of this series of samples calcined at 773 K. Noticeably, the intensity of the broad band at 969 cm^{-1} attributed to the polymerized molybdenum species decreases, and on the contrary the relative intensity of the band around 835 and 642 cm^{-1} increases with the increase of the loading amount of NiO. In addition, a broad shoulder band around 901 cm^{-1} is detected after adding NiO and it has also been observed in the spectra of MoO_3/Ni_2Zr samples (cf. Fig. 8).

It may seem appropriate to relate the above Raman results with a new surface species formed by the interaction between the dispersed molybdenum and nickel oxide species on t-ZrO_2. With the increase of NiO loading, the dispersed Ni^{2+} ions on this modified zirconia finally reach

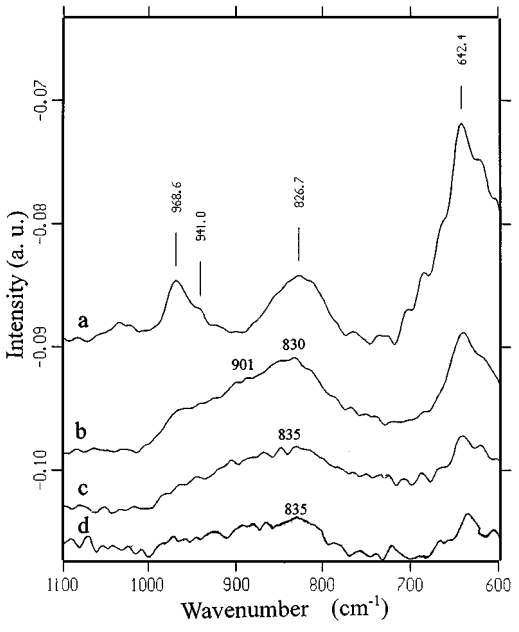

FIG. 11. Raman spectra of NiO/Mo_1Zr samples calcined at 773 K with different amounts of NiO loadings (Ni^{2+} ions/nm^2 t-ZrO_2: (a) 0 (Mo_1Zr), (b) 2.5, (c) 4.5, and (d) 7.0.

saturation, at which point the atom ratio of Mo to Ni is nearly 1 : 1. After this limit further addition of NiO will lead to the formation of crystalline NiO, but no $NiMoO_4$ phase has been detected. The absence of $NiMoO_4$ phase implies that the interaction of the surface molybdenum species with zirconia is stronger than that with NiO. The above behavior of the NiO/Mo_1Zr sample is different from that in the Ni–Mo–γ-Al_2O_3 system (26). In the case of Ni–Mo–γ-Al_2O_3 samples, at low NiO loading the nickel and molybdenum oxide species are well dispersed on the surface without mutual interactions, whereas at high NiO content, $NiMoO_4$ phase is formed by the interaction between the supported species. Similar results are also obtained in the NiO/Mo_2Zr samples, as shown in Fig. 12. By adding NiO to the Mo_2Zr sample, the changes of the individual peaks and the shape of the spectra thus formed are all similar to those observed in Fig. 11 and discussed in the previous section. The small difference is that for the Mo_2Zr sample, 2.5 Ni^{2+} ions/nm^2 t-ZrO_2 is enough for the ratio of surface species of Ni^{2+} to Mo^{6+} to become close to 1 : 1. To further increase the loading amount of NiO within a certain limit, Ni^{2+} ions still can disperse on the surface as an independent species. As the loading amount of molybdenum oxide on Mo_2Zr is 2.2 Mo^{6+} ions/nm^2 t-ZrO_2 only about half that of Mo_1Z, there are more vacant sites available on the surface of Mo_2Zr as compared to Mo_1Zr. In fact, the dispersion capacity of NiO on Mo_2Zr measured by XRD quantitative analysis is 6.6 Ni^{2+} ions/nm^2 t-ZrO_2, as shown in Fig. 5, and the result is in good agreement with the prediction of the incorporation model.

The Raman spectra of these two series of samples calcined at different temperatures are also measured and shown in Figs. 13A and 13B, respectively. No significantly different effect of the calcination temperature has been observed, and thus the dispersion states of the Ni^{2+} and Mo^{6+} appear to be independent of the calcination temperature at least in the range of 723–823 K.

The DR spectra of NiO/MoO_3-modified t-ZrO_2 samples are shown in Figs. 14 and 15. Since spectra of the two series of samples are similar in shape, the results can be discussed together. With the increase of NiO loading, the ligand charge transfer band at 265 nm attributed to monomolybdate species increases and the LMTC band between 290 and 300 nm of the surface polymolybdate species decreases correspondingly. These observations suggest the transformation of the polymolybdate species to the monomolybdate species by adding NiO. In the visible region, in low NiO loading samples (Figs. 14b and 14c), only a weak and broad band between 670 and 740 nm and a weak shoulder at 415 nm are observed, suggesting that Ni^{2+} ions might locate in an environment similar to the distorted octahedral coordination (7, 43) and probably in an octahedron with a missing corner (44, 45). With the increase of NiO loading, the band between 670 and 740 nm becomes strong and narrow, and a new adsorption band at 395 nm is present in the spectrum of high loading samples (Fig. 14e), indicating the formation of bulk NiO phase. Similar discussions can be applied to NiO/Mo_2Zr samples shown in Fig. 15. In short, the Raman and DR spectroscopic results of the above two series of samples suggest the formation of a surface

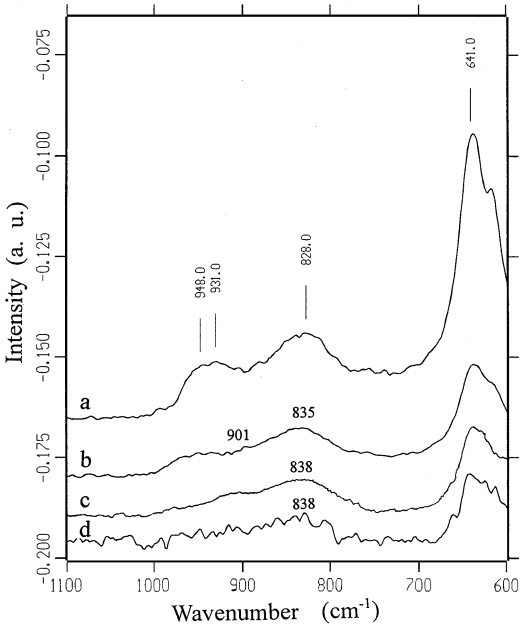

FIG. 12. Raman spectra of NiO/Mo_2Zr samples calcined at 773 K with different amounts of NiO loadings (Ni^{2+} ions/nm^2 t-ZrO_2: (a) 0 (Mo_2Zr), (b) 1.4, (c) 2.5, and (d) 5.0.

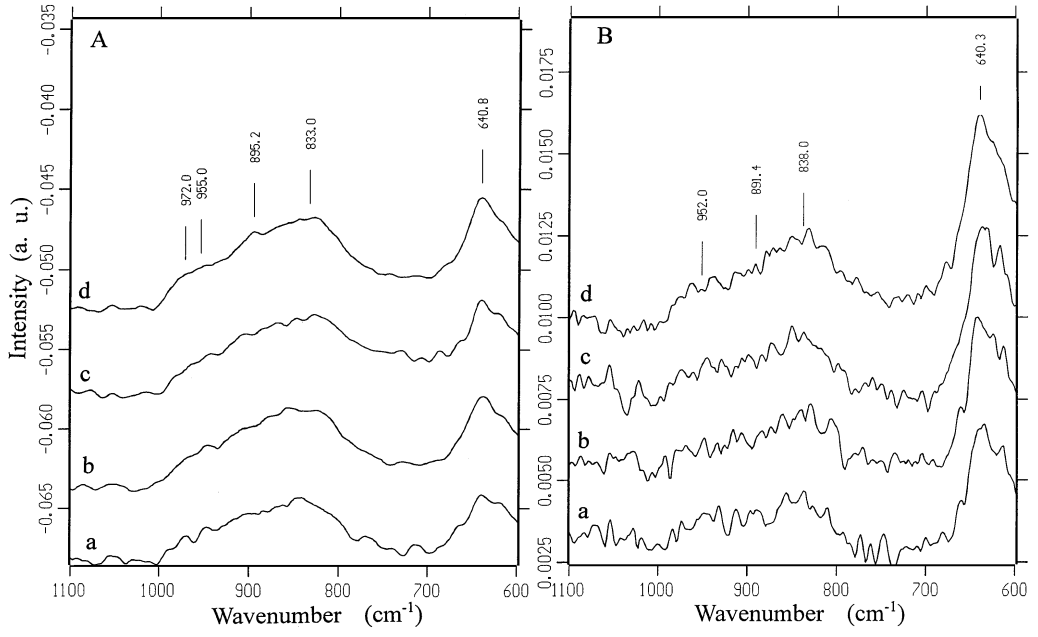

FIG. 13. Raman spectra of NiO/MoO_3-modified t-ZrO_2 samples calcined at different temperatures (K): (a) 673, (b) 723, (c) 773, and (d) 823. (A) NiO supported on Mo_1Zr with a loading of 4.5 Ni^{2+} ions/nm^2 t-ZrO_2 and (B) NiO supported on Mo_2Zr with a loading of 5.0 Ni^{2+} ions/nm^2 t-ZrO_2.

interaction species of molybdenum and nickel oxides on the surface of t-ZrO_2. The surface species might have a Mo to Ni ratio similar to that of bulk $NiMoO_4$, and the Mo^{6+} and Ni^{2+} ions are located in environments similar to those of tetrahedrally and octahedrally coordinated, respectively.

CONCLUSIONS

1. Experimental results of the dispersion of MoO_3 on t-ZrO_2 and NiO-modified t-ZrO_2 supports and of the dispersion of NiO on t-ZrO_2 and MoO_3-modified t-ZrO_2 supports

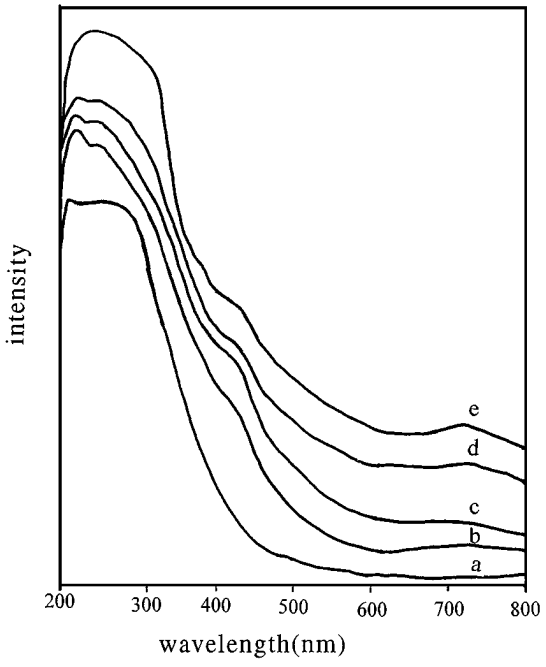

FIG. 14. UV–visible diffuse reflectance spectra of NiO/Mo_1Zr samples calcined at 773 K with different amounts of NiO loadings (Ni^{2+} ions/nm^2 t-ZrO_2: (a) 0 (Mo_1Zr), (b) 2.5, (c) 4.5, (d) 7.0, and (e) 9.7.

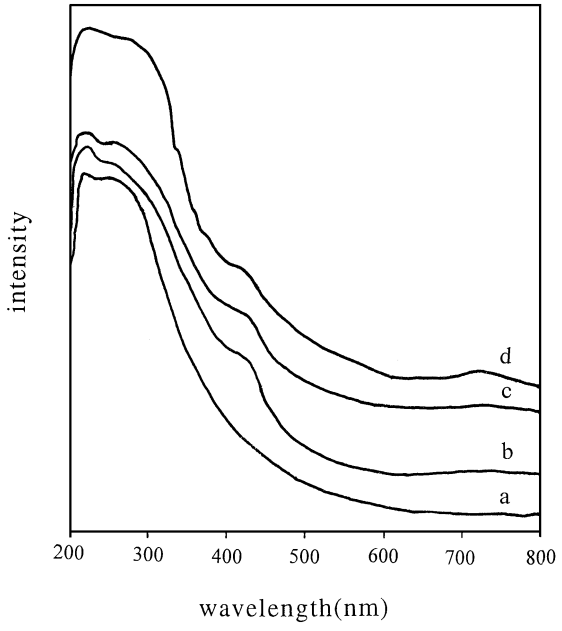

FIG. 15. UV–visible diffuse reflectance spectra of NiO/Mo_2Zr samples calcined at 773 K with different amounts of NiO loadings (Ni^{2+} ions/nm^2 t-ZrO_2: (a) 0 (Mo_2Zr) (b) 2.5, (c) 5.0, and (d) 8.4.

have demonstrated the importance of the surface structure of the support on the dispersion and the nature of the support metal oxides.

2. For t-ZrO_2-supported MoO_3 system, LRS and UV–visible DRS results indicate the formation of monomolydate and polymolybate species in samples of low and high MoO_3 loadings, respectively. Raman spectra of MoO_3/t-ZrO_2 samples are significantly different from those of MoO_3 supported on monoclinic zirconia (32). Due to the strong interaction of the dispersed molybdenum species with the support, the terminal Mo=O Raman stretch bands of the distorted mono- and polymolybdate species are shifted to 932 and 975 cm^{-1} respectively, as compared to their corresponding solution spectra.

3. In t-ZrO_2-supported NiO–MoO_3 binary oxides systems, the loading order of the oxides is critical for the species formed on the surface. Adding MoO_3 to the NiO-modified t-ZrO_2 support, at temperatures around 723 K the dispersion capability of MoO_3 is related to the amount of NiO preloaded, and no interaction between the oxide species has been detected. However, if the calcination temperature increases to 773 K, a $NiMoO_4$ phase is then formed in the above samples. On the contrary, no evidence to show the presence of the $NiMoO_4$ phase if the loading sequence of the oxide is inverted, i.e., when NiO is added to a MoO_3-modified t-ZrO_2 support. Although in the latter case the supported Ni^{2+} ions can incorporate into the residual vacant sites on the MoO_3-modified t-ZrO_2 support, a molybdenum and nickel oxide interaction species might exist on the surface.

4. The interaction of MoO_3 with t-ZrO_2 is stronger than that with NiO, and the interaction of MoO_3 with NiO is stronger than that of NiO with t-ZrO_2. The dispersion state of MoO_3 on the NiO-modified t-ZrO_2 samples depends obviously on the calcination temperature, whereas it has no significant effect on the dispersion of NiO on the MoO_3-modified t-ZrO_2 samples, at least in the range of 673 to 823 K.

REFERENCES

1. Haber, J., "The Role of Molybdenum in Catalysis." Climax Molybdenum Co., Ann Arbor, MI, 1981.
2. Segawa, K., Wachs, I. E., *in* "Characterization of Catalytic Materials" (I. E. Wachs, Ed.), p. 72. Butterworth–Heinemann, Boston, 1992.
3. Bartlett, J. R., *in* "Spectroscopy of Inorganic-Based Materials" (R. J. H. Clark and R. E. Hester, Eds.), p. 187. Wiley, New York, 1987.
4. Han, O. H., Lin, C. Y., Sustache, N., McMillan, M., Carruthers, J. D., Zilm, K. W., and Haller, G. L., *Appl. Catal. A* **98**, 195 (1993).
5. Stencel, J. M., *in* "Raman Spectroscopy for Catalysis," p. 51. Van Nostrand–Reinhold, New York, 1990.
6. Knözinger, H., and Jeziorowski, H., *J. Phys. Chem*. **82**, 2002 (1978).
7. Jeziorowski, H., and Knözinger, H., *J. Phys. Chem*. **83**, 1166 (1979).
8. Wang, L., and Hall, W. K., *J. Catal.* **66**, 251 (1980).
9. Wang, L., and Hall, W. K., *J. Catal.* **83**, 242 (1983).
10. Jeziorowski, H., Knözinger, H., Grange, P., and Gajardo, P., *J. Phys. Chem*. **84**, 1825 (1980).
11. Kohler, S. D., Ekerdt, J. G., Kim, D. S., and Wachs, I. E., *Catal. Lett.* **16**, 231 (1992).
12. Williama, C. C., Ekerdt, J. G., Jehng, J. M., Hardcastle, F. D., and Wachs, I. E., *J. Phys. Chem*. **95**, 8791 (1991).
13. Chen, Y., and Zheng, L. F., *Catal. Lett.* **12**, 51 (1992).
14. Xie, Y. C., and Tang, Y. Q., *Adv. Catal.* **37**, 1 (1990).
15. Chen, Y., Zheng, L. F., Lin, J. F., and Jin, Y. S., *in* "Catalytic Science and Technology" (S. Yoshida, N. Takezawa, and T. Ono, Eds.), Vol. 1, p. 291. Kodansha, Tokyo, 1990.
16. Chen, Y., Dong, L., Jin, Y. S., Xu, B., and Ji, W. J., *in* "Studies in Surface Science and Catalysis" (J. W. Hightower, W. N. Delgass, E. Iglesia, and A. T. Bell, Eds.), Vol. 101, p. 1293. Elsevier, Baltimore, 1996.
17. Burggraf, L. W., Leyden, D. E., Chin, R. L., and Hercules, D. M., *J. Catal.* **78**, 360 (1982).
18. Rodrigo, L., Adnot, A., Roberge, P. C., and Kaliaguine, S., *J. Catal.* **105**, 4175 (1987).
19. Hamon, D., Vrinat, M., Breysse, M., Duyand, B., Jebrouni, M., Roubin, M., Magnoux, P., and Des Courieres, T., *Catal. Today* **10**, 613 (1991).
20. Matsuoka, Y., Niwa, M., and Murakami, Y., *J. Phys. Chem*. **94**, 1477 (1990).
21. Ono, T., Miyata, H., and Kubokawa, Y., *J. Chem. Soc. Faraday Trans.* **83**, 1761 (1987).
22. Miyata, H., Tokuda, S., Ono, T., Ohno, T., and Hatayama, F., *J. Chem. Soc. Faraday Trans.* **86**, 2291 (1990).
23. Wu, M., and Hercules, D. M., *J. Phys. Chem*. **83**, 2003 (1979).
24. Chin, R., and Hercules, D. M., *J. Phys. Chem*. **86**, 360 (1982).
25. Jeziorowski, H., Knözinger, H., Taglaur, E., and Vogdt, C., *J. Catal.* **80**, 286 (1983).
26. Dufresne, P., Payen, E., Grimblot, J., and Bonnelle, J. P., *J. Phys. Chem*. **85**, 2344 (1981).
27. Ahuja, S. P., Derrien, M. L., and LePage, J. F., *Ind. Eng. Chem. Prod. Res. Dev.* **9**, 272 (1970).
28. Topsøe, H., Clausen, B. S., Burriesci, N., Candia, R., and Morup, *in* "Preparation of Catalysts II" (B. Delmon, P. A. Jacobs, and G. Poncelet, Eds.), p. 479. Elsevier, Amsterdam, 1979.
29. Cheng, C. Pm, and Schrader, G. L., *J. Catal.* **60**, 276 (1979).
30. Ng, K. Y. S., and Gular, E., *J. Catal.* **92**, 340 (1985).
31. Li, W., Zhang, W. Z., and Yin, Y. Q., *in* "7th National Conference on Catalysis (China)," p. 364. Dalian, 1994.
32. Hu, H., and Wachs, I. E., *J. Phys. Chem*. **99**, 10897 (1995).
33. Kim, D. S., Segawa, K., Soeya, T., and Wachs, I. E., *J. Catal.* **136**, 539 (1992).
34. Dong, L., and Chen, Y., *J. Chem. Soc. Faraday Trans.* **92**, 4589 (1996).
35. Hirata, T., Asari, E., and Kitajima, M., *J. Solid State Chem*. **110**, 201 (1994).
36. Miata, H., Tokuda, S., and Ono, T., *J. Chem. Soc. Faraday Trans.* **86**, 2291 (1990).
37. Zhao, B. Y., Ma, H. Y., and Tang, Y. Q., *Chinese J. Catal.* **16**, 177 (1995).
38. Anderson, J. R., "Structure of Metallic Catalysis," p. 62. Academic Press, London/New York/San Francisco, 1975.
39. Morterra, C., Cerrato, G., Ferroni, L., and Montanaro, L., *Mater. Chem. Phys.* **37**, 243 (1994).
40. Giordano, N., Bart, J. C. J., Vaghi, A., Castellan, A., and Martinotti, G., *J. Catal.* **36**, 81 (1975).
41. Afanasiev, P., Geantet, C., and Breysse, M., *J. Catal.* **153**, 17 (1995).
42. Brito, J. L., and Laine, J., *Appl. Catal.* **72**, 13 (1991).
43. Abart, J., Delgado, E., Ertl, G., Jeziorowski, H., Knozinger, H., Thiele, N., and Wang, X. Z., *Appl. Catal.* **2**, 155 (1982).
44. Berger, P. A., and Roth, J. F., *J. Phys Chem*. **71**, 4307 (1967).
45. Liu, Z., J., W. J., Dong, L., and Chen, Y., *J. Catal.* **172**, 243 (1997).